Sliding-Mode Based Output-Feedback Control of Multivariable Systems via Youla Parametrization

Richard Seeber, Stefan Koch, Martin Horn

***Abstract*—A nonlinear multivariable control scheme for linear time-invariant plants is presented that is capable of rejecting unmatched disturbances which are sufficiently often differentiable. It is based on the Youla parametrization in state space. Robust exact sliding-mode differentiators are employed for the realization of improper Youla parameters. Implementation complexity is optimized by minimizing the total number of required differentiator states. The resulting closed loop is shown to be input-to-state stable with respect to arbitrary bounded disturbances. Simulations and experimental results from a four-tank system corroborate the results.**

***Index Terms*—Sliding mode control; Linear systems; Differentiation; Robust control**

I. Introduction

Robust control of multivariable systems is an important and active area of research. One way to design such robust controllers is via sliding-mode control, see e.g. [1], [2]. For multivariable systems, in particular, several such approaches rely on the differentiation of outputs or output errors obtained from linear observers [3], [4]. When this differentiation is performed using the robust exact sliding-mode differentiator [5], exact reconstruction and full rejection of a wide class of disturbances can, in theory, be achieved.

Several differentiator-based sliding-mode approaches are found in [4], [6], [3], [7]. Thereof, [6], [7] study exact state and disturbance reconstruction by means of differentiation. In particular, [6] solves the problem by means of a minimal number of differentiations, while [7] designs an observer that requires no differentiability assumptions for the disturbance. The corresponding control design problem—stabilizing the plant and rejecting the disturbance by using the reconstructed information—is solved in [4], [3]. All of those approaches assume the disturbance to be matched, however, i.e., to act on the system in the same channel as the control signal. Unmatched disturbances are considered in [8], [9], [10]. However, all of these approaches require system transformations and, apart from [9], also impose additional restrictions on the transformed system such as strong observability.

The present paper presents a new, unified approach for output regulation based on sliding-mode disturbance reconstruction and rejection. The approach is based on the Youla parametrization [11] of stabilizing controllers. Starting from an ideal, but improper linear Youla parameter, a sliding-mode based realization of that parameter is developed. The resulting nonlinear Youla parameter is shown to yield an input-to-state stable closed loop, which can completely reject disturbances that are sufficiently often differentiable.

The *main contribution* of the present approach is a novel approach to solve the exact output regulation problem in the presence of *unmatched disturbances* by combining the Youla parametrization with sliding mode differentiators. In particular, unmatched disturbances are automatically translated—in the context of the considered output regulation problem—to differentiability requirements for the disturbance. Compared to [9], the approach avoids separate, explicit disturbance reconstruction and cancellation by handling both problems in a combined way, and does not need subspace decompositions or involved system transformations. Rather, it requires only transfer function manipulations which are straighforward to apply. Moreover, it is proven that the proposed approach *minimizes the cumulative differentiator order*[1], i.e., the total number of derivatives of scalar signals that need to be calculated during the implementation. In the context of the control problem, this improves on the results of [6], where the total number of vector-valued differentiations is minimized but, as pointed out in Remark 1 therein, fewer differentiations may sometimes be sufficient for some components of the vector.

The combination of Youla parametrization and sliding-mode control has only scarcely been studied in literature, see [12], [13], [14] for some of the few occurences. In [12], a Youla parametrization of a sliding-mode controller is presented. However, the resulting disturbance rejection performance is equivalent to that of the linear controller. In [13], a sliding-mode controller is added to a two degree-of-freedom control scheme, similar to the one considered in the present paper, but only first-order sliding-mode control is used. The use of a sliding mode observer is suggested as one possibility to obtain the states in [14], where the Youla parametrization is also used to obtain a stabilizing controller. However, none of these contributions provide a technique to achieve full disturbance rejection using robust exact sliding-mode based differentiation, as it is done in the present paper by means of a minimum number of differentiators.

Section II introduces the considered problem and briefly recapitulates the state-space form of the Youla parametrization presented in [15], [16]. Section III first uses linear techniques to design an ideal Youla parameter that, however, can not be realized as a linear state-space model. Then, a realization for this parameter is shown using a minimal number of

The authors are with the Christian Doppler Laboratory for Model Based Control of Complex Test Bed Systems, Institute of Automation and Control, Graz University of Technology, Graz, Austria.

The financial support by the Christian Doppler Research Association, the Austrian Federal Ministry for Digital and Economic Affairs and the National Foundation for Research, Technology and Development is gratefully acknowledged.

[1]A control scheme using m differentiators with orders $k_1, \dots, k_m$ is understood to have a cumulative differentiator order of $\sum_{i=1}^{m} k_i$.

sliding-mode based robust exact differentiators. Section IV proves input-to-state stability of the closed loop and states requirements for the disturbance signal that guarantee full disturbance rejection. An academic example in Section V, as well as a simulation example and experimental results in Section VI show the practical viability of the proposed approach. Section VII provides concluding remarks and gives a brief outlook.

Notation: Matrices and vectors are written as boldface uppercase and boldface lowercase letters, respectively. For scalar y and $p \geq 0$, the abbreviations $\lfloor y \rceil^p = |y|^p \operatorname{sign}(y)$ and $\lfloor y \rceil^0 = \operatorname{sign}(y)$ are used; when applied to vectors, these operations are understood to be applied component-wise. The Laplace transform and its inverse are denoted by $\mathcal{L}$ and $\mathcal{L}^{-1}$, respectively. Typically, the variable s is added as an argument to signify either the Laplace transform of a vector-valued signal, such as $\mathbf{y}(s)$, or a transfer function matrix, such as $\mathbf{Q}(s)$. When writing dynamic systems, $\dot{\mathbf{x}}$ denotes the time derivative of $\mathbf{x}$, and time dependence is typically omitted wherever it is clear from context.

II. Problem Statement

Consider a linear time invariant plant

$$\dot{\mathbf{x}} = \mathbf{A}\mathbf{x} + \mathbf{B}\mathbf{u} + \mathbf{F}\mathbf{w}, \qquad \mathbf{y} = \mathbf{C}\mathbf{x} \tag{1}$$

with state $\mathbf{x} \in \mathbb{R}^n$, control input $\mathbf{u} \in \mathbb{R}^l$, disturbance $\mathbf{w} \in \mathbb{R}^p$, output $\mathbf{y} \in \mathbb{R}^m$, and constant parameter matrices $\mathbf{A}, \mathbf{B}, \mathbf{C}, \mathbf{F}$. It is assumed that $l \geq m \geq p$ holds, and that the matrices $\mathbf{B}, \mathbf{C}, \mathbf{F}$ have maximal rank. Moreover, the plant is assumed to be minimum phase with respect to $\mathbf{u}$ and $\mathbf{y}$, and strongly detectable with respect to $\mathbf{w}$ and $\mathbf{y}$. More formally, the following assumption is made:

Assumption 1: The plant parameters $\mathbf{A} \in \mathbb{R}^{n\times n}$, $\mathbf{B} \in \mathbb{R}^{n\times l}$, $\mathbf{C} \in \mathbb{R}^{m\times n}$, $\mathbf{F} \in \mathbb{R}^{n\times p}$ with $l \geq m \geq p$ satisfy

$$\operatorname{rank}\begin{bmatrix}\mathbf{A}-\lambda\mathbf{I} & \mathbf{B}\\ \mathbf{C} & \mathbf{0}\end{bmatrix} = n+m, \quad \operatorname{rank}\begin{bmatrix}\mathbf{A}-\lambda\mathbf{I} & \mathbf{F}\\ \mathbf{C} & \mathbf{0}\end{bmatrix} = n+p \tag{2}$$

for all $\lambda \in \mathbb{C}_{\geq 0}$.

For this plant, consider an observer-based state-feedback controller of the form

$$\dot{\hat{\mathbf{x}}} = \mathbf{A}\hat{\mathbf{x}} + \mathbf{B}\mathbf{u} + \mathbf{L}(\mathbf{y} - \mathbf{C}\hat{\mathbf{x}}) \tag{3a}$$
$$\mathbf{u} = -\mathbf{K}\hat{\mathbf{x}} \tag{3b}$$

with constant $\mathbf{K}$ and $\mathbf{L}$ designed such that $\mathbf{A} - \mathbf{B}\mathbf{K}$ and $\mathbf{A} - \mathbf{L}\mathbf{C}$ are Hurwitz matrices. Starting from this controller, all controllers that stabilize the (unperturbed) plant may be obtained by means of the so-called Youla parametrization [15], [16]. In state space, this parametrization is obtained by filtering the observer innovation $\tilde{\mathbf{y}} = \mathbf{y} - \mathbf{C}\hat{\mathbf{x}}$ and adding the filter's output $\tilde{\mathbf{u}}$ to the control input. The parametrized controller is given by

$$\dot{\hat{\mathbf{x}}} = \mathbf{A}\hat{\mathbf{x}} + \mathbf{B}\mathbf{u} + \mathbf{L}\tilde{\mathbf{y}}, \tag{4a}$$
$$\tilde{\mathbf{y}} = -\mathbf{C}\hat{\mathbf{x}} + \mathbf{y}, \tag{4b}$$
$$\mathbf{u} = -\mathbf{K}\hat{\mathbf{x}} + \tilde{\mathbf{u}}, \tag{4c}$$

and the Youla parameter is the system that computes $\tilde{\mathbf{u}}$ from $\tilde{\mathbf{y}}$. A block diagram of the parametrized controller is shown in Fig. 1. It is worth pointing out that the controller (4) with a linear Youla parameter may be represented by a linear fractional transform (LFT) in frequency domain, cf. e.g. [17]. It is well-known that, by appropriate choice of the Youla parameter, different optimal controllers may be obtained.

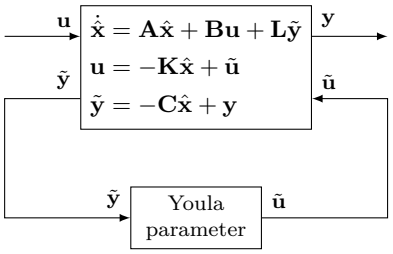

Fig. 1. Structure of the parametrized controller (4)

The goal of this paper is to use sliding-mode techniques for realizing an ideal Youla parameter which permits complete rejection of the disturbance.

III. Design of Youla Parameter

The design is divided in two steps. First, an ideal linear Youla parameter is computed. Then, sliding-mode techniques and robust exact differentiation are used to approximate its behavior. Stability and disturbance rejection properties of the closed loop are afterwards derived in the next section.

A. Ideal Youla Parameter

For the first step, assume that $\tilde{\mathbf{u}}(s) = \mathbf{Q}(s)\tilde{\mathbf{y}}(s)$ holds in Laplace domain with some transfer-function matrix $\mathbf{Q}(s)$. Introducing the observer error $\tilde{\mathbf{x}} = \mathbf{x} - \hat{\mathbf{x}}$, the closed-loop system with input $\tilde{\mathbf{u}}$ and output $\tilde{\mathbf{y}}$ may be written as

$$\dot{\mathbf{x}} = (\mathbf{A} - \mathbf{B}\mathbf{K})\mathbf{x} + \mathbf{B}\mathbf{K}\tilde{\mathbf{x}} + \mathbf{B}\tilde{\mathbf{u}} + \mathbf{F}\mathbf{w}, \tag{5a}$$
$$\dot{\tilde{\mathbf{x}}} = (\mathbf{A} - \mathbf{L}\mathbf{C})\tilde{\mathbf{x}} + \mathbf{F}\mathbf{w}, \tag{5b}$$
$$\tilde{\mathbf{y}} = \mathbf{C}\tilde{\mathbf{x}}. \tag{5c}$$

Transforming into Laplace domain, with initial conditions $\mathbf{x}(0) = \tilde{\mathbf{x}}(0) = \mathbf{0}$, yields

$$\begin{aligned}(s\mathbf{I} - \mathbf{A} + \mathbf{B}\mathbf{K})\mathbf{x}(s) &= \big(\mathbf{B}\mathbf{K} + \mathbf{B}\mathbf{Q}(s)\mathbf{C}\big)\tilde{\mathbf{x}}(s) + \mathbf{F}\mathbf{w}(s),\\ (s\mathbf{I} - \mathbf{A} + \mathbf{L}\mathbf{C})\tilde{\mathbf{x}}(s) &= \mathbf{F}\mathbf{w}(s),\end{aligned} \tag{6}$$

and by solving for $\tilde{\mathbf{x}}(s)$ and $\mathbf{x}(s)$, the transfer relation between disturbance $\mathbf{w}$ and output $\mathbf{y} = \mathbf{C}\mathbf{x}$ is obtained as

$$\begin{aligned}\mathbf{y}(s) &= \mathbf{C}(s\mathbf{I} - \mathbf{A} + \mathbf{B}\mathbf{K})^{-1}\\ &\quad\cdot\Big[\big(\mathbf{B}\mathbf{K} + \mathbf{B}\mathbf{Q}(s)\mathbf{C}\big)(s\mathbf{I} - \mathbf{A} + \mathbf{L}\mathbf{C})^{-1} + \mathbf{I}\Big]\mathbf{F}\mathbf{w}(s),\\ &= \Big[\mathbf{G}_1(s)\mathbf{Q}(s)\mathbf{G}_2(s) + \mathbf{G}_3(s) + \mathbf{G}_1(s)\mathbf{G}_4(s)\Big]\mathbf{w}(s)\end{aligned} \tag{7}$$

with

$$\mathbf{G}_1(s) = \mathbf{C}(s\mathbf{I} - \mathbf{A} + \mathbf{B}\mathbf{K})^{-1}\mathbf{B}, \tag{8a}$$
$$\mathbf{G}_2(s) = \mathbf{C}(s\mathbf{I} - \mathbf{A} + \mathbf{L}\mathbf{C})^{-1}\mathbf{F}, \tag{8b}$$
$$\mathbf{G}_3(s) = \mathbf{C}(s\mathbf{I} - \mathbf{A} + \mathbf{B}\mathbf{K})^{-1}\mathbf{F}, \tag{8c}$$
$$\mathbf{G}_4(s) = \mathbf{K}(s\mathbf{I} - \mathbf{A} + \mathbf{L}\mathbf{C})^{-1}\mathbf{F}. \tag{8d}$$

The construction of an ideal Youla parameter that achieves complete disturbance rejection is based on the following auxiliary lemma.

Proposition 1: Suppose that Assumption 1 holds and that the matrices $\mathbf{A}-\mathbf{BK}$ and $\mathbf{A}-\mathbf{LC}$ are Hurwitz. Then, the transfer function matrices $\mathbf{G}_1(s)$ and $\mathbf{G}_2(s)$ defined in (8) have a stable (but not necessarily proper) left-inverse $\mathbf{G}_1^{-1}(s)$ and right-inverse $\mathbf{G}_2^{-1}(s)$, respectively.

Proof: It is sufficient to show that the matrices $\mathbf{G}_1(s)$ or $\mathbf{G}_2(s)$ are left- or right-invertible, respectively, for every $s\in\mathbb{C}_{\geq 0}$, which implies that their inverses have no poles in the right complex half-plane. This is now shown for $\mathbf{G}_2(s)$; the proof for $\mathbf{G}_1(s)$ is analogous after transposition. Fix $\lambda\in\mathbb{C}_{\geq 0}$ and suppose to the contrary that $\mathbf{G}_2(\lambda)\in\mathbb{C}^{m\times p}$ is not right-invertible. Then, there exists a vector $\mathbf{q}\in\mathbb{C}^p$ such that

$$\mathbf{G}_2(\lambda)\mathbf{q}=\mathbf{C}(\lambda\mathbf{I}-\mathbf{A}+\mathbf{LC})^{-1}\mathbf{F}\mathbf{q}=\mathbf{0} \tag{9}$$

Denote $\mathbf{v}=(\lambda\mathbf{I}-\mathbf{A}+\mathbf{LC})^{-1}\mathbf{F}\mathbf{q}$, and note that $\mathbf{v}$ is well-defined because $\mathbf{A}-\mathbf{LC}$ is Hurwitz. Then, since $\mathbf{C}\mathbf{v}=\mathbf{0}$,

$$\mathbf{0}=\mathbf{F}\mathbf{q}-(\lambda\mathbf{I}-\mathbf{A}+\mathbf{LC})\mathbf{v}=(\mathbf{A}-\lambda\mathbf{I})\mathbf{v}+\mathbf{F}\mathbf{q} \tag{10}$$

which implies

$$\begin{bmatrix}\mathbf{A}-\lambda\mathbf{I} & \mathbf{F}\\ \mathbf{C} & \mathbf{0}\end{bmatrix}\begin{bmatrix}\mathbf{v}\\ \mathbf{q}\end{bmatrix}=\mathbf{0}. \tag{11}$$

This contradicts Assumption 1, which requires this matrix to have full column rank for all $\lambda\in\mathbb{C}_{\geq 0}$. ∎

As a consequence of this lemma, an ideal Youla parameter that nullifies the influence of the disturbance on the output may be computed as

$$\mathbf{Q}(s)=-\big[\mathbf{G}_4(s)+\mathbf{G}_1(s)^{-1}\mathbf{G}_3(s)\big]\mathbf{G}_2(s)^{-1}. \tag{12}$$

This transfer function matrix is improper, because the numerator degree of its entries generally exceeds the degree of the denominator. In general, it may be written as

$$\mathbf{Q}(s)=\mathbf{H}(s)+\mathbf{J}(s) \tag{13}$$

where $\mathbf{H}(s)$ is a biproper transfer-function matrix and $\mathbf{J}(s)$ is a polynomial matrix of dimension $l\times m$.

B. Sliding-Mode Based Realization

The part $\mathbf{H}(s)$ may be realized by means of a linear state-space model using standard techniques, see, e.g. [18]. In order to realize the transfer behavior of the polynomial matrix $\mathbf{J}(s)$, a sliding-mode based differentiation approach is proposed.

To that end, $\mathbf{J}(s)$ is written as

$$\mathbf{J}(s)=\mathbf{J}_0+\mathbf{J}_1 s+\mathbf{J}_2 s^2+\ldots+\mathbf{J}_k s^k, \tag{14}$$

where $\mathbf{J}_j$ $(j=1,\ldots,k)$ are constant coefficient matrices and k denotes the highest degree of the polynomials occuring in $\mathbf{J}(s)$. Performing an inverse Laplace transform of the expression $\mathbf{J}(s)\tilde{\mathbf{y}}(s)$ yields in time-domain

$$\mathcal{L}^{-1}(\mathbf{J}(s)\tilde{\mathbf{y}}(s))=\mathbf{J}_0\tilde{\mathbf{y}}+\mathbf{J}_1\frac{\mathrm{d}\tilde{\mathbf{y}}}{\mathrm{d}t}+\ldots+\mathbf{J}_k\frac{\mathrm{d}^k\tilde{\mathbf{y}}}{\mathrm{d}t^k}. \tag{15}$$

This expression suggests that up to k derivatives of each of the m outputs need to be computed. A naive implementation would therefore require m parallel k-th order differentiators, i.e., a cumulative differentiator order of $m\cdot k$.

C. Minimization of Cumulative Differentiator Order

The following approach minimizes the cumulative order of the required differentiators. To achieve this, linear combinations of $\tilde{\mathbf{y}}$ are first determined, which are then fed to differentiators of varying orders. These linear combinations and the required differentiator orders are determined by the following algorithm: For each $j=k,k-1,\ldots,0$ in descending order, compute orthogonal rectangular matrices $\mathbf{P}_j$, $\mathbf{V}_j$ and invertible diagonal matrices $\mathbf{\Sigma}_j$ according to the following steps:

1) Define
$$\tilde{\mathbf{J}}_j=\mathbf{J}_j-\mathbf{J}_j\sum_{r=j+1}^{k}\mathbf{V}_r\mathbf{V}_r^{\mathrm{T}}, \tag{16}$$
i.e., orthogonally decompose $\mathbf{J}_j$ into components parallel and orthogonal to $\mathbf{V}_{j+1},\mathbf{V}_{j+2},\ldots,\mathbf{V}_k$ as
$$\mathbf{J}_j=\tilde{\mathbf{J}}_j+\mathbf{J}_j\mathbf{V}_{j+1}\mathbf{V}_{j+1}^{\mathrm{T}}+\ldots+\mathbf{J}_j\mathbf{V}_k\mathbf{V}_k^{\mathrm{T}}. \tag{17}$$
2) Perform a singular value decomposition of $\tilde{\mathbf{J}}_j$ to obtain $\mathbf{P}_j\in\mathbb{R}^{l\times\alpha_j}$, $\mathbf{V}_j\in\mathbb{R}^{m\times\alpha_j}$, and $\mathbf{\Sigma}_j\in\mathbb{R}^{\alpha_j\times\alpha_j}$ according to
$$\tilde{\mathbf{J}}_j=\mathbf{P}_j\mathbf{\Sigma}_j\mathbf{V}_j^{\mathrm{T}}, \tag{18}$$
where α_j is the number of non-zero singular values, i.e., $\alpha_j=\operatorname{rank}\tilde{\mathbf{J}}_j$. Note that $\mathbf{V}_j$, $\mathbf{P}_j$, and $\mathbf{\Sigma}_j$ may be empty (zero-column) matrices if all singular values are zero; in this case, step three can be skipped for this value of j.
3) Unless $j=0$, apply a sliding-mode based differentiator of order j to the expression $\mathbf{V}_j^{\mathrm{T}}\tilde{\mathbf{y}}$, i.e.,
$$\begin{aligned}
\dot{\boldsymbol{\zeta}}_{j,0}&=\kappa_{j,0}\left\lfloor\mathbf{V}_j^{\mathrm{T}}\tilde{\mathbf{y}}-\boldsymbol{\zeta}_{j,0}\right\rceil^{\frac{j}{j+1}}+\boldsymbol{\zeta}_{j,1}\\
\dot{\boldsymbol{\zeta}}_{j,1}&=\kappa_{j,1}\left\lfloor\mathbf{V}_j^{\mathrm{T}}\tilde{\mathbf{y}}-\boldsymbol{\zeta}_{j,0}\right\rceil^{\frac{j-1}{j+1}}+\boldsymbol{\zeta}_{j,2}\\
&\vdots\\
\dot{\boldsymbol{\zeta}}_{j,j-1}&=\kappa_{j,j-1}\left\lfloor\mathbf{V}_j^{\mathrm{T}}\tilde{\mathbf{y}}-\boldsymbol{\zeta}_{j,0}\right\rceil^{\frac{1}{j+1}}+\boldsymbol{\zeta}_{j,j}\\
\dot{\boldsymbol{\zeta}}_{j,j}&=\kappa_{j,j}\left\lfloor\mathbf{V}_j^{\mathrm{T}}\tilde{\mathbf{y}}-\boldsymbol{\zeta}_{j,0}\right\rceil^{0}
\end{aligned} \tag{19}$$
with constant parameters $\kappa_{j,0},\ldots,\kappa_{j,j}$ and componentwise application of the operator $\lfloor\cdot\rceil^p$ to obtain in finite time the derivatives
$$\boldsymbol{\zeta}_{j,1}=\frac{\mathrm{d}\mathbf{V}_j^{\mathrm{T}}\tilde{\mathbf{y}}}{\mathrm{d}t},\quad\ldots,\quad\boldsymbol{\zeta}_{j,j}=\frac{\mathrm{d}^j\mathbf{V}_j^{\mathrm{T}}\tilde{\mathbf{y}}}{\mathrm{d}t^j}. \tag{20}$$
Note that (19) contributes $j\operatorname{rank}\mathbf{V}_j=j\alpha_j$ to the cumulative differentiator order.

Remark 1: For SISO plants, i.e., $l=m=p=1$, the algorithm yields $\mathbf{V}_k=1$, while $\mathbf{V}_{k-1},\ldots,\mathbf{V}_0$ are empty.

Remark 2: It is worth to remark that in step 3), instead of the differentiator (19), a robust exact filtering differentiator as proposed in [19] may also be used to obtain the time derivatives $\boldsymbol{\zeta}_{j,1},\ldots,\boldsymbol{\zeta}_{j,j}$. Doing so may improve the differentiation accuracy in the presence of random measurement noise in practice.

By following the steps of the algorithm, it is obvious that the expression $\mathbf{J}_j\frac{\mathrm{d}^j\tilde{\mathbf{y}}}{\mathrm{d}t^j}$ may be computed as

$$\mathbf{J}_j\frac{\mathrm{d}^j\tilde{\mathbf{y}}}{\mathrm{d}t^j}=\mathbf{P}_j\mathbf{\Sigma}_j\frac{\mathrm{d}^j\mathbf{V}_j^{\mathrm{T}}\tilde{\mathbf{y}}}{\mathrm{d}t^j}+\sum_{r=j+1}^{k}\mathbf{J}_j\mathbf{V}_r\frac{\mathrm{d}^j\mathbf{V}_r^{\mathrm{T}}\tilde{\mathbf{y}}}{\mathrm{d}t^j} \tag{21}$$

from the outputs of the resulting differentiators. Further insight into the algorithm and a simplification of this expression is obtained using the following lemma, which shows that the algorithm yields an orthogonal decomposition of the vector space $\mathbb{R}^m$ of the signal $\tilde{\mathbf{y}}$.

Lemma 1: Consider orthogonal matrices $\mathbf{V}_j \in \mathbb{R}^{m\times\alpha_j}$ as obtained using the presented algorithm, with $\alpha_j = \operatorname{rank}\mathbf{V}_j$ for $j = 0,\dots,k$. Then, the columns of the matrix

$$\mathbf{M} = \begin{bmatrix}\mathbf{V}_0 & \mathbf{V}_1 & \mathbf{V}_2 & \dots & \mathbf{V}_k\end{bmatrix} \tag{22}$$

are orthogonal, i.e., $\mathbf{M}^{\mathrm{T}}\mathbf{M} = \mathbf{I}$.

Remark 3: This lemma shows that the sum $\sum_{j=1}^{k}\alpha_j$ cannot exceed k. If it is equal to k, then $\mathbf{M}$ is invertible; otherwise, if it is less than k, then parts of the signal $\tilde{\mathbf{y}}$, which lie in the nullspace of $\mathbf{M}$, are not needed to realize $\mathbf{J}(s)$.

Remark 4: Using this lemma and relation (16), one straightforwardly obtains that

$$\mathbf{J}_j\mathbf{V}_j = \big(\tilde{\mathbf{J}}_j + \mathbf{J}_j\sum_{r=j+1}^{k}\mathbf{V}_r\mathbf{V}_r^{\mathrm{T}}\big)\mathbf{V}_j = \tilde{\mathbf{J}}_j\mathbf{V}_j = \mathbf{P}_j\mathbf{\Sigma}_j \tag{23}$$

Hence, (21) may be rewritten more concisely as

$$\mathbf{J}_j\frac{\mathrm{d}^j\tilde{\mathbf{y}}}{\mathrm{d}t^j} = \sum_{r=j}^{k}\mathbf{J}_j\mathbf{V}_r\boldsymbol{\zeta}_{r,j}. \tag{24}$$

Proof: Since all $\mathbf{V}_j$ are orthogonal matrices by construction, it suffices to prove the following statement: for all j and all $q > j$, $\mathbf{V}_j^{\mathrm{T}}\mathbf{V}_q = \mathbf{0}$. The proof is done by induction over j, starting with $j = k$, in which case the statement is trivially true.

Suppose that the statement is true for all $j \geq i$, i.e., $\mathbf{V}_j^{\mathrm{T}}\mathbf{V}_q = \mathbf{0}$ for all $q > j \geq i$. To see that it is then also true for $j = i-1$, note that for all $q > i-1$ one has

$$\sum_{r=i}^{k}\mathbf{V}_r\mathbf{V}_r^{\mathrm{T}}\mathbf{V}_q = \sum_{r=i}^{q}\mathbf{V}_r\mathbf{V}_r^{\mathrm{T}}\mathbf{V}_q + \sum_{r=q+1}^{k}\mathbf{V}_r(\mathbf{V}_q^{\mathrm{T}}\mathbf{V}_r)^{\mathrm{T}} = \mathbf{V}_q. \tag{25}$$

Consequently, (16) and (18) yield

$$\mathbf{0} = \tilde{\mathbf{J}}_{i-1}\mathbf{V}_q = \mathbf{P}_{i-1}\mathbf{\Sigma}_{i-1}\mathbf{V}_{i-1}^{\mathrm{T}}\mathbf{V}_q, \tag{26}$$

which implies $\mathbf{V}_{i-1}^{\mathrm{T}}\mathbf{V}_q = \mathbf{0}$, because $\mathbf{P}_{i-1}\mathbf{\Sigma}_{i-1}$ has full column rank. ∎

Let now $(\mathbf{\Lambda}, \mathbf{\Pi}, \mathbf{\Gamma}, \mathbf{\Theta})$ be a minimal state-space representation of the transfer function matrix $\mathbf{H}(s)$. The realized Youla parameter is then obtained from (15) and (24) as

$$\dot{\mathbf{z}} = \mathbf{\Lambda}\mathbf{z} + \mathbf{\Pi}\tilde{\mathbf{y}} \tag{27a}$$

$$\tilde{\mathbf{u}} = \mathbf{\Gamma}\mathbf{z} + (\mathbf{\Theta} + \mathbf{J}_0)\tilde{\mathbf{y}} + \sum_{j=1}^{k}\sum_{r=j}^{k}\mathbf{J}_j\mathbf{V}_r\boldsymbol{\zeta}_{r,j} \tag{27b}$$

Fig. 2 depicts a block diagram representation of this system.

The following theorem shows that the presented realization (27) of the ideal Youla parameter (12) minimizes the cumulative differentiator order.

Theorem 1: Consider the realization of $\mathbf{J}(s)$ obtained using the presented algorithm in the form of matrices $\mathbf{P}_j \in \mathbb{R}^{l\times\alpha_j}$, $\mathbf{V}_j \in \mathbb{R}^{m\times\alpha_j}$, and $\mathbf{\Sigma}_j \in \mathbb{R}^{\alpha_j\times\alpha_j}$, with $\alpha_j = \operatorname{rank}\mathbf{V}_j$ for $j = 1,\dots,k$. Then, the cumulative differentiator order is given by $\sum_{j=1}^{k} j\alpha_j$ and it is minimal among all possible differentiator-based realizations of $\mathbf{J}(s)$.

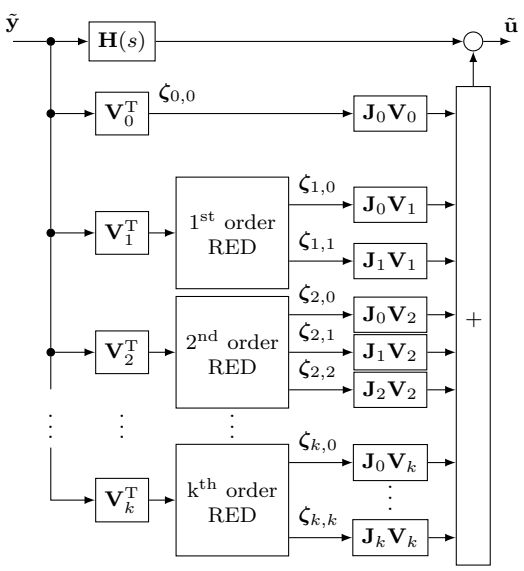

Fig. 2. Sliding-mode based realization of the ideal Youla parameter using robust exact differentiators (REDs) with minimal cumulative order

Proof: The expression for the cumulative differentiator order follows from the fact that the j-th differentiator has input dimension α_j and differentiator order j. It remains to be shown that this cumulative order is minimal. Let $r \in [0,k]$ be an arbitrary integer and $\mathbf{v} \in \mathbb{R}^{\alpha_r}$ be an arbitrary vector. Consider the signal $\tilde{\mathbf{y}}(t) = \mathbf{V}_r\mathbf{v}t^r$; the corresponding output of $\mathbf{J}(s)$ at $t = 0$ is given by

$$\left(\mathbf{J}_0\tilde{\mathbf{y}} + \ldots + \mathbf{J}_k\frac{\mathrm{d}^k\tilde{\mathbf{y}}}{\mathrm{d}t^k}\right)\Bigg|_{t=0} = \mathbf{J}_r\mathbf{V}_r\mathbf{v} = \mathbf{P}_r\mathbf{\Sigma}_r\mathbf{v} \tag{28}$$

Due to the orthogonality of the matrices $\mathbf{V}_j$ shown in Lemma 1, all differentiator inputs except the signal $\mathbf{V}_r^{\mathrm{T}}\tilde{\mathbf{y}}(t) = \mathbf{v}t^r$ are zero. Hence, the structure of the other differentiators has no influence on the present output, and it suffices to show that neither the signal dimension α_r nor the order r of the differentiator for $\mathbf{V}_r^{\mathrm{T}}\tilde{\mathbf{y}}$ can be reduced without altering the obtained output signal.

To see this, suppose to the contrary that another correct realization requires a derivative of order r only for a signal of reduced dimension, i.e., for $\mathbf{M}\mathbf{V}_r^{\mathrm{T}}\tilde{\mathbf{y}}$ with some $\mathbf{M} \in \mathbb{R}^{c\times\alpha_j}$, $c < \alpha_j$. This implies existence of a non-zero vector $\mathbf{v}$ such that $\mathbf{M}\mathbf{v} = \mathbf{0}$. Then, for the considered structure of $\tilde{\mathbf{y}}(t)$, the differentiator input $\mathbf{M}\mathbf{V}_r^{\mathrm{T}}\tilde{\mathbf{y}}(t) = \mathbf{M}\mathbf{v}t^r$ and hence also its output are zero for all t. The output $\mathbf{P}_r\mathbf{\Sigma}_r\mathbf{v}$ in (28), however, is non-zero for all non-zero $\mathbf{v}$, because $\mathbf{P}_r\mathbf{\Sigma}_r$ by construction has full column rank. This contradiction proves minimality of the cumulative differentiator order for r-th order differentiation of the signal $\mathbf{V}_r^{\mathrm{T}}\tilde{\mathbf{y}}$ and, since r is arbitrary, for the entire realization. ∎

IV. Stability Considerations

In the following, two stability properties of the closed loop are proven. First, input-to-state stability with respect to

arbitrary, bounded disturbances is shown. Subject to some additional differentiability requirements for the disturbance, full disturbance rejection at the output, i.e., asymptotic convergence of the output to zero, is then proven.

A. Input-to-State Stability

The following theorem shows that, by appropriately tuning the differentiators in order to achieve finite-time stability of differentiation errors, the closed loop is input-to-state stable with respect to the disturbance $\mathbf{w}$.

Theorem 2: Suppose that Assumption 1 holds and that the matrices $\mathbf{A}-\mathbf{BK}$ and $\mathbf{A}-\mathbf{LC}$ are Hurwitz. Consider the closed loop obtained by the interconnection of the plant (1), observer-based state-feedback controller (4), and the realization (19), (27) of the ideal Youla parameter (12). Then, for any given positive parameter values of $\kappa_{j,j}$ $(j=0,\dots,k)$ there exist further positive parameters $\kappa_{j,r}$ $(j=0,\dots,k;\ r=0,\dots,j-1)$ for the differentiators, such that the closed loop with disturbance input $\mathbf{w}$ is input-to-state stable.

Remark 5: If L_j is a Lipschitz constant of the j-th derivative of the respective signal to be differentiated, i.e., if

$$\left\| \frac{\mathrm{d}^{j+1}\mathbf{V}_j^{\mathrm{T}}\tilde{\mathbf{y}}(t)}{\mathrm{d}t^{j+1}} \right\|_\infty \leq L_j, \tag{29}$$

holds for all t, then a common choice for $\kappa_{j,j}$ is $1.1L_j$; for the selection of the other parameters, cf. [5], [20].

Proof: Looking at (5), one can see that the observer error dynamics (5b)–(5c) with input $\mathbf{w}$ and output $\tilde{\mathbf{y}}$ is input-to-state stable (ISS), because $\mathbf{A}-\mathbf{LC}$ is Hurwitz. Furthermore, the dynamics of the plant state (5a) with inputs $\tilde{\mathbf{x}}$, $\tilde{\mathbf{u}}$ and $\mathbf{w}$ are ISS, since $\mathbf{A}-\mathbf{BK}$ is Hurwitz. Thus, it suffices to show that the realization of the Youla parameter with input $\tilde{\mathbf{y}}$ and output $\tilde{\mathbf{u}}$ is input-to-state stable. Input-to-state stability of the overall closed-loop system then follows from the fact that it is a cascade interconnection of input-to-state stable systems.

The realization of the transfer function matrix $\mathbf{H}(s)$ is ISS due to the stable invertability of $\mathbf{G}_1$ and $\mathbf{G}_2$. The only remaining dynamics are the differentiators (19), whose inputs are linear combinations of the observer output error $\tilde{\mathbf{y}}$. According to [20, Proposition 2], these also are ISS for appropriate gains $\kappa_{j,r}$ $(j=0,\dots,k;\ r=0,\dots,j)$. Due to the homogeneity property of the differentiator, these gains can always be rescaled such that all $\kappa_{j,j}$ have desired values without altering the stability properties. ∎

B. Disturbance Rejection

Similar to [4], the presented sliding-mode based realization of an ideal Youla parameter permits to suppress a certain class of disturbances. The class of disturbances, which can be rejected, is defined by certain differentiability requirements. The following theorem provides conditions, which guarantee asymptotic stability of the closed loop despite the disturbance.

Theorem 3: Suppose that Assumption 1 holds, that the matrices $\mathbf{A}-\mathbf{BK}$ and $\mathbf{A}-\mathbf{LC}$ are Hurwitz, and let $W\geq 0$. Consider the controller obtained by the interconnection of the observer-based state-feedback controller (4) and the realization (19), (27) of the ideal Youla parameter (12). Then, there exist parameters $\kappa_{j,r}$ $(j=0,\dots,k;\ r=0,\dots,j-1)$, such that the output $\mathbf{y}(t)$ tends to zero, i.e., $\lim_{t\to\infty}\mathbf{y}(t)=\mathbf{0}$, whenever the disturbance $\mathbf{w}$ is such that $\|\mathbf{w}(t)\|_\infty \leq W$ for all t, and that for all integers j,r with $1\leq j\leq r\leq k$ the linear combinations of the disturbance $\mathbf{w}$ given by

$$\boldsymbol{\psi}_{r,j} = \mathbf{V}_r^{\mathrm{T}}\mathbf{C}(\mathbf{A}-\mathbf{LC})^{j-1}\mathbf{F}\mathbf{w} \tag{30}$$

are $r-j+1$ times differentiable and that all derivatives also are uniformly bounded with respect to time with bound W.

Proof: Since $(\mathbf{A}-\mathbf{LC})$ is Hurwitz and $\mathbf{w}$ is uniformly bounded, also $\tilde{\mathbf{x}}$ is uniformly bounded due to (5b). Then, the $(r+1)$-th time derivative of the input $\mathbf{V}_r^{\mathrm{T}}\tilde{\mathbf{y}}$ to the r-th (and thus r-th order) differentiator, as depicted in Fig. 2,

$$\frac{\mathrm{d}^{r+1}\mathbf{V}_r^{\mathrm{T}}\tilde{\mathbf{y}}}{\mathrm{d}t^{r+1}} = \mathbf{V}_r^{\mathrm{T}}(\mathbf{A}-\mathbf{LC})^{r+1}\tilde{\mathbf{x}} + \sum_{j=1}^{r}\frac{\mathrm{d}^{r-j+1}\boldsymbol{\psi}_{r,j}}{\mathrm{d}t^{r-j+1}}, \tag{31}$$

exists and is also uniformly bounded. Hence, given a uniform bound $W\geq 0$, there exist parameters $\kappa_{j,r}>0$ such that all differentiator errors converge to zero in finite time.

Consider now any closed-loop trajectory and let T be a corresponding upper bound for the convergence times of all differentiators. Then, in the state-space realization (27),

$$\mathbf{J}_0\tilde{\mathbf{y}} + \sum_{j=1}^{k}\sum_{r=j}^{k}\mathbf{J}_j\mathbf{V}_r\boldsymbol{\zeta}_{r,j} = \mathbf{J}_0\tilde{\mathbf{y}} + \mathbf{J}_1\frac{\mathrm{d}\tilde{\mathbf{y}}}{\mathrm{d}t} + \ldots + \mathbf{J}_k\frac{\mathrm{d}^k\tilde{\mathbf{y}}}{\mathrm{d}t^k} \tag{32}$$

holds for $t\geq T$ by construction. As a consequence, the closed loop behaves like a linear, time-invariant system for $t\geq T$ and the trajectory can be split into two additive components, which are denoted by the indices $(\cdot)^{(1)}$ and $(\cdot)^{(2)}$ in the following. Let the splitting be performed such that $\mathbf{w}^{(2)}=\mathbf{w}-\mathbf{w}^{(1)}$ is differentiable, $\tilde{\mathbf{x}}^{(2)}(T)=\mathbf{0}$ holds, and, moreover, that $\mathbf{w}^{(2)}$ and all its derivatives up to order $k-2$ vanish at $t=T$ whereas $\mathbf{w}^{(1)}$ and all derivatives of the signals $\boldsymbol{\psi}_{r,j}^{(1)}$ defined in (30) up to order $r-j$ tend to zero for $t\to\infty$.

For the first trajectory, the vanishing $\mathbf{w}^{(1)}$ and the Hurwitz property of $\mathbf{A}-\mathbf{LC}$ in (5b) allow to conclude that also $\lim_{t\to\infty}\tilde{\mathbf{x}}^{(1)}(t)=\mathbf{0}$. Furthermore, all derivatives of $\tilde{\mathbf{y}}^{(1)}$ that are relevant in computing $\tilde{\mathbf{u}}^{(1)}$ vanish by virtue of the vanishing $\boldsymbol{\psi}_{r,j}^{(1)}$ and a similar computation as in (31), and hence also $\lim_{t\to\infty}\tilde{\mathbf{u}}^{(1)}(t)=\mathbf{0}$. Consequently, $\lim_{t\to\infty}\mathbf{x}^{(1)}(t)=\mathbf{0}$ follows from (5a) and the fact that $\mathbf{A}-\mathbf{BK}$ is Hurwitz. For the second trajectory, the vanishing initial condition $\tilde{\mathbf{x}}^{(2)}(T)$ along with differentiability and vanishing derivatives of $\mathbf{w}^{(2)}$ at $t=T$ imply that $\tilde{\mathbf{y}}^{(2)}$ and its derivatives up to order $k-1$ exist and are zero at $t=T$. Computing the Laplace transform of (32) for[2] $t\geq T$ hence yields $\mathbf{J}(s)\tilde{\mathbf{y}}^{(2)}(s)$. Therefore,

$$\tilde{\mathbf{u}}^{(2)}(s) = \mathbf{Q}(s)\tilde{\mathbf{y}}^{(2)}(s) \tag{33}$$

holds in Laplace domain with the ideal Youla parameter $\mathbf{Q}(s)$ and consequently $\mathbf{y}^{(2)}(s)=\mathbf{0}$ is obtained by design, which implies $\mathbf{y}^{(2)}(t)=\mathbf{0}$ for $t\geq T$. The claim now follows from the fact that, for $t\geq T$, $\mathbf{y}(t)=\mathbf{y}^{(1)}(t)+\mathbf{y}^{(2)}(t)$ holds, and $\mathbf{y}^{(1)}(t)$ tends to zero whereas $\mathbf{y}^{(2)}(t)$ is equal to zero. ∎

[2]The Laplace transform of a signal $f(t)$ for $t\geq T$ is understood to be computed as $\int_T^\infty f(t)e^{-s(t-T)}\,\mathrm{d}t$.

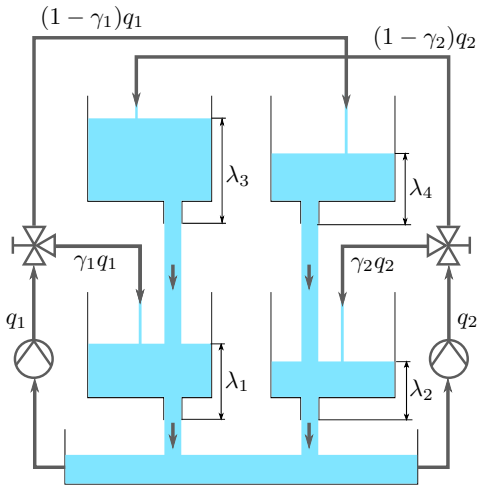

Fig. 3. Schematic of the considered four-tank system.

TABLE I
SYSTEM PARAMETERS.

Parameter	Description	Value	Unit
a_1	drain area	0.67	cm^2
a_2	drain area	0.74	cm^2
a_3	drain area	0.26	cm^2
a_4	drain area	0.32	cm^2
A_ν	tank bottom surface area	69.68	cm^2
$\tilde{h}_1$, $\tilde{h}_3$	socket height	10.1	cm
$\tilde{h}_2$, $\tilde{h}_4$	socket height	8.1	cm
k_1	control gain	0.3622	$cm^3/(Vs)$
k_2	control gain	0.3190	$cm^3/(Vs)$
γ_1, γ_2	flow ratio	0.7	-
$\bar{\lambda}_1$	nominal operating point	31.75	cm
$\bar{\lambda}_2$	nominal operating point	25.73	cm
$\bar{\lambda}_3$	nominal operating point	23.62	cm
$\bar{\lambda}_4$	nominal operating point	16.47	cm
$\bar{v}_1$,$\bar{v}_4$	nominal operating point	6	V

V. Academic SISO Example

As a simple illustrative example, consider the SISO plant

$$\dot{x}_1 = x_2 + cw, \qquad \dot{x}_2 = u + w, \qquad y = x_1 + x_2 \tag{34}$$

wherein $c \geq 0$ is a known constant. Design the parametrized observer-based state-feedback controller as

$$\dot{\hat{x}}_1 = \hat{x}_2 + \ell_1 \tilde{y}, \qquad \tilde{y} = -\hat{x}_1 - \hat{x}_2 + y, \tag{35a}$$
$$\dot{\hat{x}}_2 = u + \ell_2 \tilde{y}, \qquad u = -k_1 \hat{x}_1 - k_2 \hat{x}_2 + \tilde{u}. \tag{35b}$$

From (12)-(13), the polynomial $\mathbf{J}(s) = -s-(\ell_1+\ell_2+k_2-1)$ and transfer function $\mathbf{H}(s) = \frac{(k_2-k_1-1)(\ell_1-1)}{s+1}$ are obtained. According to Remark 1, $\mathbf{V}_0$ is not present and $\mathbf{V}_1 = 1$. Theorem 3 requires w to be differentiable only once regardless of whether the disturbance is matched or unmatched. The Youla parameter, finally, is given by the first-order differentiator realizing $\mathbf{J}(s)$ and the linear system realizing $\mathbf{H}(s)$ as

$$\dot{\zeta}_{2,0} = \kappa_{2,0} \lfloor \tilde{y} - \zeta_{2,0} \rceil^{\frac{1}{2}} + \zeta_{2,1}, \tag{36a}$$
$$\dot{\zeta}_{2,1} = \kappa_{2,1} \lfloor \tilde{y} - \zeta_{2,0} \rceil^{0} \tag{36b}$$
$$\dot{z} = -z + (k_2 - k_1 - 1)(\ell_1 - 1)\tilde{y} \tag{36c}$$
$$\tilde{u} = -(\ell_1 + \ell_2 + k_2 - 1)\zeta_{2,0} - \zeta_{2,1} + z. \tag{36d}$$

VI. Application to Multivariable Four-Tank System

The interacting four-tank system, see e.g., [21] which is shown schematically in Fig. 3 is used to demonstrate the application of the proposed sliding mode based control approach. The system consists of four tanks which are arranged as shown in the illustration. Each tank has a rectangular bottom surface of area A_ν, $\nu = 1, \ldots, 4$ and there is a drain on the bottom. The area of the drain and the hight of the drain socket differs from tank to tank and is denoted by a_ν and $\tilde{h}_\nu$, respectively. The tanks are arranged so that water flows from the upper tank into the tank directly below and from the lower tanks into a collecting reservoir. Two pumps are used to pump water from the collecting reservoir back to the tanks. In particular, each pump delivers water to a lower and the opposing upper tank. The ratio of the volumetric flow rate between the lower and the corresponding upper tank can be adjusted by a valve. The ratio is denoted by γ_μ with $\gamma_\mu \in [0, 1]$ and $\mu = 1, 2$ in the following. The opening width of the drain of each tank can in principle also be adjusted via valves.

The control goal is to regulate the levels in the lower two tanks. As control inputs the voltages applied to the two pumps are considered. In this regard, the system features two inputs and two outputs. The filling level in each tank, excluding the socket height, can be measured with a sampling time of 0.01 seconds. MATLAB/Simulink is used to implement and deploy the algorithm to the control hardware. It is noteworthy, that in the experiment the minimum pump voltage was limited in order to ensure that the hoses to the upper two tanks are always filled with water and thus avoid transport delays.

Using the proposed approach a controller is designed based on a mathematical system model in the following. The system dynamics are modeled by the sixth order nonlinear system

$$\frac{\mathrm{d}\lambda_1}{\mathrm{d}t} = -\frac{a_1}{A_1}\sqrt{2g\lambda_1} + \frac{a_3}{A_1}\sqrt{2g\lambda_3} + \frac{\gamma_1}{A_1}q_1, \tag{37a}$$
$$\frac{\mathrm{d}\lambda_2}{\mathrm{d}t} = -\frac{a_2}{A_2}\sqrt{2g\lambda_2} + \frac{a_4}{A_2}\sqrt{2g\lambda_4} + \frac{\gamma_2}{A_2}q_2, \tag{37b}$$
$$\frac{\mathrm{d}\lambda_3}{\mathrm{d}t} = -\frac{a_3}{A_3}\sqrt{2g\lambda_3} + \frac{(1-\gamma_2)}{A_3}q_2 - \frac{1}{A_3}w_1, \tag{37c}$$
$$\frac{\mathrm{d}\lambda_4}{\mathrm{d}t} = -\frac{a_4}{A_4}\sqrt{2g\lambda_4} + \frac{(1-\gamma_1)}{A_4}q_1 - \frac{1}{A_4}w_2, \tag{37d}$$
$$\tau\frac{\mathrm{d}\omega_1}{\mathrm{d}t} = -\omega_1 + v_1, \quad q_1 = k_1\omega_1, \quad h_1 = \lambda_1 - \tilde{h}_1 \tag{37e}$$
$$\tau\frac{\mathrm{d}\omega_2}{\mathrm{d}t} = -\omega_2 + v_2, \quad q_2 = k_2\omega_2, \quad h_2 = \lambda_2 - \tilde{h}_2 \tag{37f}$$

see, [22]. Therein the state variables λ_ν, represent the total filling level of each tank, i.e., including the socket (see Fig. 3), q_μ are the inlet flow rates and g is the gravity constant. The dynamics of the pump are modeled by a first order lag with time constant τ and gain k_μ where the state variable ω_μ represents the pump speed. The pump supply voltage is denoted by v_μ. The variables w_1 and w_2 in (37c), (37d) denote unknown external disturbances, i.e., unknown inflows

and outflows into the upper two tanks. The system outputs h_μ are the filling levels of the lower two tanks minus the heights of the outlet sockets $\tilde{h}_\mu$. The system parameters are summarized in Table I.

In the following, the proposed control approach is applied to regulate the levels h_1 and h_2. To that end, the nonlinear system (37) is linearized about the nominal operating point $\lambda_\nu = \bar{\lambda}_\nu$, $v_\mu = \bar{v}_\mu$ from Table I with $w_\mu = 0$. The resulting linear time invariant model is in the form (1) with parameters

$$\mathbf{A} = \begin{bmatrix} -\frac{1}{T_1} & 0 & \frac{A_3}{A_1 T_3} & 0 & \frac{\gamma_1}{A_1} & 0 \\ 0 & -\frac{1}{T_2} & 0 & \frac{A_4}{A_2 T_4} & 0 & \frac{\gamma_2}{A_2} \\ 0 & 0 & -\frac{1}{T_3} & 0 & 0 & \frac{(1-\gamma_2)}{A_3} \\ 0 & 0 & 0 & -\frac{1}{T_4} & \frac{(1-\gamma_1)}{A_4} & 0 \\ 0 & 0 & 0 & 0 & -\frac{1}{\tau} & 0 \\ 0 & 0 & 0 & 0 & 0 & -\frac{1}{\tau} \end{bmatrix},$$

$$\mathbf{B} = \begin{bmatrix} 0 & 0 \\ 0 & 0 \\ 0 & 0 \\ 0 & 0 \\ \frac{k_1}{\tau} & 0 \\ 0 & \frac{k_2}{\tau} \end{bmatrix}, \quad \mathbf{F} = \begin{bmatrix} 0 & 0 \\ 0 & 0 \\ -\frac{1}{A_3} & 0 \\ 0 & -\frac{1}{A_4} \\ 0 & 0 \\ 0 & 0 \end{bmatrix}, \quad \mathbf{C} = \begin{bmatrix} 1 & 0 \\ 0 & 1 \\ 0 & 0 \\ 0 & 0 \\ 0 & 0 \\ 0 & 0 \end{bmatrix}^{\mathrm{T}} \tag{38}$$

where $T_\nu = \frac{A_\nu}{a_\nu}\sqrt{\frac{2\bar{\lambda}_\nu}{g}}$. It is noteworthy, that for $(\gamma_1 + \gamma_2) > 1$ the linear system is minimum phase, see, e.g., [22].

The state feedback controller

$$\mathbf{K} = \begin{bmatrix} 1.046 & 0.015 & 0.068 & 0.045 & 0.460 & 0.015 \\ 0.003 & 0.975 & 0.061 & 0.093 & 0.015 & 0.394 \end{bmatrix} \tag{39}$$

as well as the observer gains

$$\mathbf{L} = \begin{bmatrix} 0.485 & 0.001 & 0.047 & 0.013 & 0.025 & 0 \\ 0.001 & 0.474 & 0.010 & 0.048 & 0 & 0.022 \end{bmatrix}^{\mathrm{T}} \tag{40}$$

are computed using the LQR approach. With this particular parameters, the polynomial matrix $\mathbf{J}(s)$ in (13) takes the form (14) with

$$\mathbf{J}_0 = \begin{bmatrix} -4.085 & -0.015 \\ 0.021 & -4.260 \end{bmatrix}, \quad \mathbf{J}_1 = \begin{bmatrix} -9.818 & -0.015 \\ 0.021 & -10.840 \end{bmatrix},$$
$$\mathbf{J}_2 = \begin{bmatrix} -7.888 & 0 \\ 0 & -8.957 \end{bmatrix}. \tag{41}$$

Following Remark 2, the transfer behavior of $\mathbf{J}(s)$ is realized using the differentiator toolbox presented in [23] which implements the robust exact filtering differentiator published in [19]. The differentiator order is two, the filtering order is set to one and the differentiator gains are $\kappa_{2,2} = 0.015$, $\kappa_{2,1} = 0.172$, $\kappa_{2,0} = 0.735$ and $\kappa_{2,-1} = 1.4$. The differentiators are discretized using the approach discussed in [24]. The toolbox enables the real-time implementation of the differentiator at the used control hardware.

The performance of the controller is evaluated in a first step in simulation. For this purpose, the controller is applied to the non-linear model (37). The simulation is carried out in MATLAB/Simulink. The discretization step size is set to 0.01 seconds. Note that this corresponds to the sampling time

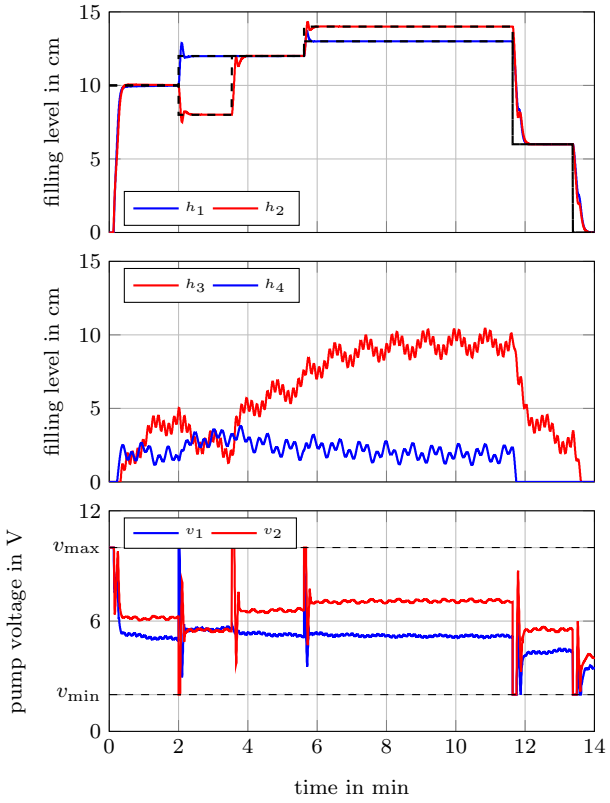

Fig. 4. Simulation results. As can be seen in the uppermost graph, the controller ensures accurate tracking of the setpoint despite the disturbances $w_1(t) = 5\sin(0.12t) + 20\sin(0.7t) + 3$ and $w_2(t) = 4\sin(0.15t) + 10\sin(0.4t) + 5$.

in the real system. The simulation results are presented in Fig. 4. The upper graph shows the evolution of the levels in the two lower tanks (red and blue solid lines) as well as the desired level (black dashed lines). The graph in the middle shows the evolution of the filling level in the upper two tanks. The pump supply voltages are plotted in the graph on the bottom. It can be seen from the upper plot that the controller is capable of driving the filling level of the two lower tanks to the desired value despite the non-vanishing disturbances, which, in this simulation is selected as $w_1(t) = 5\sin(0.12t)+20\sin(0.7t)+3$ and $w_2(t) = 4\sin(0.15t) + 10\sin(0.4t) + 5$. The filling level in the upper two tanks show an oscillating behavior which is due to the disturbances w_1, w_2 (graph in the middle). Also the control signals show an oscillating behavior after the transient phases as it counteracts the effect of the disturbance. Note that in this simulation no noise is considered in order to emphasize the disturbance rejection properties of the proposed controller, i.e. to demonstrate the asymptotic convergence in the presence of the disturbances of the filling level in the lower two tanks to the desired filling level.

The controller is applied with the same settings to the real system. The results are shown in Fig. 5, where the arrangement of the plots is the same as in Fig. 4. Also in the experiment, the controller ensures accurate tracking of the same set-point as in the simulation. In the real experiment, the robustness against measurement noise is also apparent. Furthermore, controller

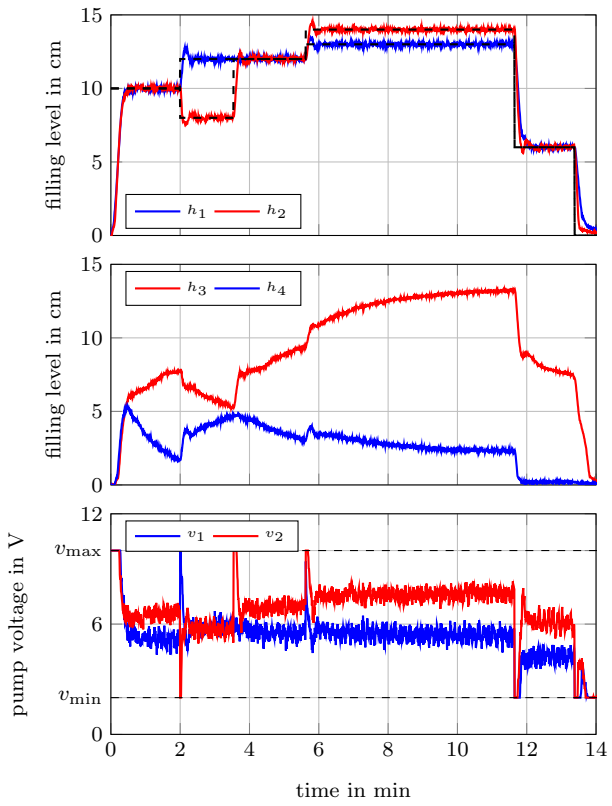

Fig. 5. Experimental results. The same controller as used in simulation is applied to the experimental setup. It can be seen, that it ensures accurate setpoint tracking.

windup is avoided, since the proposed approach inherently possesses the observer based based anti-windup property, see [25] for details.

VII. Conclusion and Outlook

By designing a sliding-mode based Youla parameter, a unified approach for differentiation-based disturbance cancellation for multivariable plants was developed. Apart from stabilizability, the only requirements for applying it are strong detectability of the plant with respect to the disturbance and asymptotic stability of the zero dynamics of the plant's output. In particular, the approach also handles unmatched disturbances and, subject to certain differentiability requirements, can fully cancel their influence on the output. Moreover, it is proven that the approach minimizes the implementation complexity in the sense that the cumulative differentiator order of the required sliding-mode differentiators is minimized. The application to a multivariable four tank system demonstrated the proposed approach's efficiacy both in simulations and experiments. In the future, the influence of additional effects such as parametric or multiplicative uncertainties in the plant model may be investigated.

References

[1] Vadim Utkin, Jürgen Guldner, and Jingxin Shi. *Sliding Mode Control in Electro-Mechanical Systems*. CRC Press, 2nd edition, 2009.

[2] Yuri B. Shtessel, Christopher Edwards, Leonid Fridman, and Arie Levant. *Sliding Mode Control and Observation*. Springer, New York, 2014.

[3] Marco Tulio Angulo, Leonid Fridman, and Arie Levant. Robust exact finite-time output based control using high-order sliding modes. *International Journal of Systems Science*, 42(11):1847–1857, 2011.

[4] Alejandra Ferreira, Francisco Javier Bejarano, and Leonid M. Fridman. Robust control with exact uncertainties compensation: With or without chattering? *IEEE Transactions on Control Systems Technology*, 19(5):969–975, 2011.

[5] Arie Levant. Robust exact differentiation via sliding mode technique. *Automatica*, 34(3):379 – 384, 1998.

[6] Francisco J. Bejarano and Leonid Fridman. High order sliding mode observer for linear systems with unbounded unknown inputs. *International Journal of Control*, 83(9):1920–1929, 2010.

[7] Markus Tranninger, Richard Seeber, Martin Steinberger, and Martin Horn. Exact state estimation for LTI-systems with non-differentiable unknown inputs. In *18th European Control Conference (ECC)*, pages 3096–3102, Naples, Italy, 2019.

[8] Alejandra Ferreira De Loza, Francisco Javier Bejarano, and Leonid Fridman. Unmatched uncertainties compensation based on high-order sliding mode observation. *International Journal of Robust and Nonlinear control*, 23(7):754–764, 2013.

[9] Francisco Javier Bejarano and Jorge Dávila. Output stabilization of linear systems with disturbances. In *Multibody Mechatronic Systems*, pages 35–43. Springer, 2015.

[10] Shihua Li, Haibin Sun, Jun Yang, and Xinghuo Yu. Continuous finite-time output regulation for disturbed systems under mismatching condition. *IEEE Transactions on Automatic Control*, 60(1):277–282, 2015.

[11] Dante C. Youla, Hamid A. Jabr, and Joseph J. Bongiorno. Modern Wiener-Hopf design of optimal controllers–part II: The multivariable case. *IEEE Transactions on Automatic Control*, 21(3):319–338, 1976.

[12] Kenichiro Nonaka. Youla-parametrization of output feedback sliding mode controller: internal stability and disturbance rejection. In *American Control Conference*, volume 1, pages 535–539, 1999.

[13] Yasutaka Fujimoto and Atsuo Kawamura. Robust servo-system based on two-degree-of-freedom control with sliding mode. *IEEE Transactions on Industrial Electronics*, 42(3):272–280, 1995.

[14] R. Galindo. Stabilisation using a stable controller and robust stability and performance. *International Journal of Control*, 81(8):1183–1194, 2008.

[15] John B. Moore, Keith Glover, and Andrew Telford. All stabilizing controllers as frequency-shaped state estimate feedback. *IEEE Transactions on Automatic Control*, 35(2):203–208, 1990.

[16] Way M. Lu, Kemin Zhou, and John C. Doyle. Stabilization of LFT systems. In *Proceedings of the 30th IEEE Conference on Decision and Control*, pages 1239–1244, 1991.

[17] Kemin Zhou, John Doyle, and Keith Glover. *Robust and Optimal Control*. Prentice-Hall, Upper Saddle River, NJ, USA, 1996.

[18] Thomas Kailath. *Linear systems*, volume 156. Prentice-Hall Englewood Cliffs, NJ, 1980.

[19] Arie Levant and Miki Livne. Robust exact filtering differentiators. *European Journal of Control*, 55:33–44, 2020.

[20] Emmanuel Cruz-Zavala and Jaime A. Moreno. Levant's arbitrary-order exact differentiator: A Lyapunov approach. *IEEE Transactions on Automatic Control*, 64(7):3034–3039, 2019.

[21] Karl Henrik Johansson and Jose Luis Rocha Nunes. A multivariable laboratory process with an adjustable zero. In *Proceedings of the 1998 American Control Conference (ACC)*, volume 4, pages 2045–2049, 1998.

[22] Edward P. Gatzke, Edward S. Meadows, Chung Wang, and Francis J. Doyle III. Model based control of a four-tank system. *Computers & Chemical Engineering*, 24(2-7):1503–1509, 2000.

[23] Benedikt Andritsch, Martin Horn, Stefan Koch, Helmut Niederwieser, Maximilian Wetzlinger, and Markus Reichhartinger. The robust exact differentiator toolbox revisited: Filtering and discretization features. In *IEEE International Conference on Mechatronics, Kashiwa, Japan*, 2021.

[24] Stefan Koch, Markus Reichhartinger, Martin Horn, and Leonid Fridman. Discrete-time implementation of homogeneous differentiators. *IEEE Transactions on Automatic Control*, 65(2):757–762, 2019.

[25] Karl Johan Astrom and Lars Rundqwist. Integrator windup and how to avoid it. In *1989 American Control Conference*, pages 1693–1698. IEEE, 1989.